Published for SISSA by Springer

Received: *July 21, 2025*
Accepted: *August 26, 2025*
Published: *September 26, 2025*

NNLO+PS double Higgs boson production with top-quark mass corrections in GENEVA

Simone Alioli,[a] **Giulia Marinelli**[b] **and Davide Napoletano**[a]

[a] *Università degli Studi di Milano-Bicocca & INFN, Piazza della Scienza 3, Milano 20126, Italy*
[b] *Deutsches Elektronen-Synchrotron DESY, Notkestr. 85, 22607 Hamburg, Germany*

E-mail: simone.alioli@unimib.it, giulia.marinelli@desy.de, davide.napoletano@unimib.it

Abstract: We present the implementation of the NNLO QCD corrections to double Higgs boson production at hadron colliders in Geneva, matched to the parton shower. We include top-quark mass effects and the resummation of large logarithms of the zero-jettiness $\mathcal{T}_0$, up to NNLL′ accuracy. This work extends our previous study, which was performed in the $m_t \to \infty$ infinite top-quark mass approximation, providing a more realistic simulation framework for Higgs boson pair production. We validate our approach against NNLO predictions by Matrix and assess the importance of mass effects comparing with our $m_t \to \infty$ previous implementation.

Keywords: Higgs Production, Higher-Order Perturbative Calculations, Parton Shower, Resummation

ArXiv ePrint: 2507.08558

https://doi.org/10.1007/JHEP09(2025)206

Contents

1 Introduction

With the upcoming High-Luminosity phase of the Large Hadron Collider (LHC), one of the most urgent tasks is to tighten the constraint of the Higgs boson trilinear coupling. While most of its properties have been precisely measured and shown to be consistent with Standard Model predictions [1–3], only loose bounds currently exist on the Higgs boson self-coupling [4].

The most important process entering the study of the Higgs boson trilinear coupling is the production of a pair of Higgs bosons, where the self-coupling appears already at leading order [5–7]. Due to its similarity to the single Higgs boson production case, higher order QCD corrections (NNLO [8, 9] and $\mathrm{N^3LO}$ [10]) have been computed in the infinite top-quark mass limit, but NLO QCD corrections including the full top-quark mass dependence are also available [11, 12]. In addition, electroweak (EW) corrections have been recently presented [13–18], as well as methods to include approximate top-quark mass corrections in higher order calculations [19–24]. Finally, NLO QCD corrections with full top-quark mass dependence have been matched to parton showers [25–27].

In this work, we extend our previous result in GENEVA ref. [28], where we presented fully differential Higgs boson pair events at NNLO accuracy in the strict $m_t \to \infty$ limit, matched to parton showers. The exact inclusion of top-quark mass effects at NNLO is extremely challenging, as the process features a heavy-quark loop already at leading order. Despite this, partial three-loops amplitudes, which are part of the full NNLO corrections, are starting to become available [29–34]. Here, we include full top-quark mass corrections at NLO and approximate mass corrections at NNLO, achieving what is usually referred to as $\mathrm{FT}_{\mathrm{approx}}$, as presented at fixed order in refs. [35, 36]. Compared to these results, our implementation includes the resummation of zero-jettiness, $\mathcal{T}_0$, at NNLL′ accuracy, as well as parton shower matching. It is important to notice, however, that in the $\mathrm{FT}_{\mathrm{approx}}$ the inclusion of the unknown mass corrections in the virtual amplitudes is done via a reweighting procedure which originates from the case of the production of a single Higgs boson in gluon fusion, where the

JHEP09(2025)206

leading order amplitude involves only a single diagram — the top-quark triangle loop. As such, there is no ambiguity on whether the reweighting of these contributions is performed at amplitude, or squared amplitude level, as they yield the same results. For di-Higgs production, this is no longer the case, as the process now comprise a resonant production channel which resembles that of the single Higgs boson and a non-resonant heavy-quark box diagram. The relative contributions of these diagrams vary across different regions of phase space, allowing for multiple, formally equivalent, choices for the reweighting, leading to different approximations. See refs. [37, 38] and references therein for more details, where various parts of the amplitudes are reweighted differently. In our case, we chose to reweight squared matrix elements, as this significantly simplifies the implementation task.

Regardless of the details of the reweighting procedure used for the contributions that are still unknown, the inclusion of top-quark mass effects plays a crucial role in achieving realistic and accurate predictions for the production of a pair of Higgs bosons. Indeed, it is widely accepted that the $m_t \to \infty$ approximation only works in a narrow region of phase space and is thus not suitable for precise phenomenological applications.

In addition to higher-order QCD corrections, recent calculations have also provided higher-order EW corrections [13, 14, 39], which are essential for reducing theoretical uncertainties. Since this process is proportional to the top-quark Yukawa coupling, it features a strong m_t scheme dependence [40], resulting in an estimated uncertainty of approximately 20% [41–43]. This can be reduced by including higher-order top-quark Yukawa corrections, both of EW [44] and QCD origin [34]. In this work, however, we neglect such effects, as our primary interest is on the effect of QCD corrections. Nonetheless, future versions of our code will need to incorporate top-quark Yukawa scheme variations, as well as at least approximate EW corrections. Another source of theoretical uncertainty arises from the treatment of bottom-quark mass corrections and of possible interference terms. To our current knowledge, the only estimates of these effects come from single Higgs boson production, where they are known to be around 5% [45, 46]. Two-loop corrections, including bottom-quark mass, which are part of the NLO corrections, have only been recently computed in the planar limit [33]. We therefore neglect bottom-quark mass effects in our calculation, treating the bottom quark as massless throughout.

Since the production of a pair of Higgs bosons is highly sensitive to the Higgs boson self-coupling, it offers the possibility to probe eventual differences with the Higgs boson potential as predicted by the Standard Model. For this purpose, this process has been heavily studied within the Standard Model Effective Theory (SMEFT) framework, including NLO QCD corrections and parton shower effects [37, 47–58].

The outline of this paper is the following. In section 2, we highlight the differences of this new implementation with respect to ref. [28], describing, in particular, the details of the reweighting procedure used to obtain the $\mathrm{FT}_{\mathrm{approx}}$ predictions. In section 3, we describe the validation of our findings and compare with results from ref. [36]. In section 4, we study the importance of the inclusion of top-quark mass effects by comparing our parton level results obtained with different treatments of the top-quark mass corrections. We then proceed to compare our best $\mathrm{FT}_{\mathrm{approx}}$ predictions at different stages of the parton shower procedure in section 5. Finally, in section 6, we report our conclusions.

JHEP09(2025)206

2 Theoretical framework and differences with $m_t \to \infty$ approximation

In this work, we extend our previously presented implementation of Higgs boson pair production process in GENEVA [28] to include top-quark mass corrections exactly up to NLO and in the $\text{FT}_{\text{approx}}$ approximation for the NNLO corrections [22, 23, 36]. We start by briefly reviewing the main features of the existing implementation, referring the reader to ref. [28] and references therein for a more comprehensive discussion of the GENEVA framework and its implementation. Here, we limit ourselves to report the main formulae that are either essential for our discussion of mass effects, or are necessary to describe our modifications. In addition to our new $\text{FT}_{\text{approx}}$ result, we also compare to our previous $m_t \to \infty$ approximation as well as to the leading order reweighted result (referred to as B-proj). These results all share the same structure. The interested reader can find all the relevant formulae for the differential cross sections at different multiplicities in eqs. (2.2)–(2.4) of ref. [28].

Calculations in the GENEVA framework are done using a resolution variable to split the phase space into resolved and unresolved QCD emissions. A common choice for this variable is the zero-jettiness $\mathcal{T}_0$ [59], which we employ in this work. In the region where the resolution variable is smaller than a given $\mathcal{T}_0^{\text{cut}} \ll Q$, we can exploit the leading power SCET factorisation theorem for this observable [60]. In particular, this allows us to perform the resummation of large logarithms of $\mathcal{T}_0^{\text{cut}}/Q$, where $Q = m_{HH}$ is the invariant mass of the Higgs boson pair system. At leading power in $\mathcal{T}_0^{\text{cut}}/m_{HH}$, we can write the differential cross section as

$$\frac{\mathrm{d}\sigma^{\text{SCET}}}{\mathrm{d}\Phi_0\,\mathrm{d}\mathcal{T}_0} = H_{gg\to HH}(Q^2,\mu) \int B_g(t_a,x_a,\mu)\, B_g(t_b,x_b,\mu)\, S_{gg}\left(\mathcal{T}_0 - \frac{t_a+t_b}{Q},\mu\right) \mathrm{d}t_a\,\mathrm{d}t_b, \quad (2.1)$$

where H stands for the hard function, while S and B for the soft and beam functions, respectively. The resummed formula is then matched to the appropriate fixed order calculation to yield predictions that are valid across the entire phase space. This is achieved in an additive approach, by summing the resummed and fixed order contributions and subtracting the appropriate fixed order expansion of the resummed contribution (resummed-expanded). Note that eq. (2.1) is identical, in form, to eq. (2.17) of ref. [28], although the exact top-quark mass dependence of the perturbative ingredients within each term does depend on the specific approximation. In the following subsections we detail these differences in the three cases considered in this work.

2.1 The $\text{FT}_{\text{approx}}$ approximation

The $\text{FT}_{\text{approx}}$ is defined by including the exact mass effects up to NLO and, where possible, also at NNLO. For NNLO contributions where the exact top-quark mass dependence is not known, the unknown terms are reweighted using the corresponding Born-level contributions with exact mass dependence [22, 23, 36].

All Born-level processes are computed with our existing OPENLOOPS [61–63] interface, which provides the exact top-quark mass dependence. These include the loop-induced leading order diagram, as well as all real and double-real corrections. Exact virtual corrections are only known up to NLO and are available through HHGRID [11, 12, 25], which provides pre-computed amplitudes on a two-dimensional grid for fixed Higgs boson and top-quark masses. These grids are then interpolated to avoid re-computation of the full two-loop

JHEP09(2025)206

integrals at every phase space point, and we have implemented a dedicated interface to access the value of these grids in GENEVA. NNLO double-virtual and real-virtual corrections are not known with full top-quark mass dependence. These are therefore reweighted by the corresponding Born matrix elements computed with exact mass dependence. Compared to the original formulae presented in eqs. (2.2)–(2.4) of ref. [28], we compute the B_0, B_1, B_2 and V_0 terms using exact top-quark mass dependence. We include leading order mass effects in the real-virtual term V_1, through the reweighting

$$V_1(\Phi_1) = V_1(\Phi_1, m_t \to \infty) \frac{B_1(\Phi_1, m_t)}{B_1(\Phi_1, m_t \to \infty)}. \tag{2.2}$$

As explained in eq. (2.27) of ref. [28], we do not need to reweight the double-virtual term W_0, as it does not contribute for $\mathcal{T}_0 > \mathcal{T}_0^{\text{cut}}$. Instead, two-loop virtual corrections are included in the two-loop hard function coefficient via eq. (2.1). The only change in the resummation part of our calculation, compared to the $m_t \to \infty$ result, lies in the top-quark mass dependence of the hard function perturbative coefficients, which encode the hard part of loop corrections. This is a consequence of the universality of the factorisation theorem: since soft and collinear modes are insensitive to the details of the hard modes that are integrated out, top-quark mass effects enter exclusively through the Wilson coefficient of the hard function. In this case, the Born and the finite part of the one-loop coefficients, which are related to $H^{(0)}$ and $H^{(1)}_{\text{fin}}$, respectively, are known exactly and obtained from OPENLOOPS [61–63] and HHGRID [11, 12, 25, 64]. However, to ensure cancellation of the slicing variable dependence, the fixed order expansion of the resummed expression must be consistent with the fixed order implementation. In particular, for $\mathcal{T}_0 > \mathcal{T}_0^{\text{cut}}$, the finite one-loop contribution $H^{(1)}_{\text{fin}}$ must be reweighted in the same way as the real-virtual term. Accordingly, the two-loop term, which appears in the finite part of the second order coefficients, $H^{(2)}_{\text{fin}}$, and $H^{(1)}_{\text{fin}}$ are thus rescaled as

$$H^{(i)}_{\text{fin}}(\Phi_0) = H^{(i)}_{\text{fin}}(\Phi_0, m_t \to \infty) \frac{B_0(\Phi_0, m_t)}{B_0(\Phi_0, m_t \to \infty)}, \quad i = 1, 2. \tag{2.3}$$

We remark that the reweighting of the top-quark mass dependence in $H^{(1)}_{\text{fin}}$ is only necessary to ensure the correct expansion of the resummed cross section and its cancellation against the V_1 contribution, which is reweighted similarly. This does not mean that the exact top-quark mass dependence at NLO coming from HHGRID is not used in our calculation, because it is still present in the fixed order part, where it enters in the virtual correction, V_0. Alternatively, one could have also included the exact $H^{(1)}_{\text{fin}}$ in the resummed part and the approximated one in the resummed-expanded. In this way one would get the exact top-quark mass dependence at NNLL′ but then the cancellation between the resummed and the resummed-expanded at large values of $\mathcal{T}_0$ would need to be enforced by hand. In the current implementation we preferred the first option, i.e. to include the exact top-quark mass dependence only at fixed order.

The relation between the Born, the finite part of the one-loop amplitudes, and the hard function coefficients can be found e.g. in refs. [28, 65]. All coefficients are then transformed to the $\overline{\text{MS}}$ scheme [65, 66] from the IR subtraction scheme in which they were originally computed. Crucially, all other terms, either in the soft and beam functions or in the evolution operators needed for the $\mathcal{T}_0$ and $\mathcal{T}_1$ resummations, remain unchanged from the $m_t \to \infty$

JHEP09(2025)206

case. This includes our choice of profile scales and the relevant transition points, see ref. [28] and references therein for more details.

Given that the loop-order of almost all matrix elements is increased by one unit in the $\mathrm{FT}_{\mathrm{approx}}$, the calculation is significantly more challenging from the numerical point of view. In particular, the treatment of the one-loop double-real matrix element $gg \to HHgg$ is notably delicate near the double limit $\mathcal{T}_0, \mathcal{T}_1 \to 0$, compared to the other approximations. The stability of double-real matrix elements near the double unresolved limit is an issue that has been noted also in ref. [36]. Their approach was to use the $m_t \to \infty$ matrix element for $gg \to HHgg$, reweighted by the massive Born matrix element in regions where at least one scalar product $\alpha_{ij} = p_i \cdot p_j / \hat{s}$ falls below a technical cut, chosen to be $\alpha_{\mathrm{cut}} = 10^{-4}$. The mapping used to project the two-parton phase space into the $gg \to HH$ kinematics is done by preserving the momenta of the two Higgs bosons, but significantly affects the incoming partons, which might no longer be along the beam directions. In our case, such procedure cannot be used, as it breaks the subtraction mechanism required for the calculation of the NLO corrections to the one-parton phase space (NLO_1). We therefore construct the approximation of the double-real matrix elements as follows

$$\mathrm{d}\sigma_{gg\to HHgg}\left(\Phi_2\right)\Big|_{\min(\alpha_{ij})<\alpha_{\mathrm{cut}}} = \mathrm{d}\sigma_{gg\to HHg}\left(\widetilde{\Phi}_1\right)\frac{\mathrm{d}\sigma^{m_t\to\infty}_{gg\to HHgg}\left(\Phi_2\right)}{\mathrm{d}\sigma^{m_t\to\infty}_{gg\to HHg}\left(\widetilde{\Phi}_1\right)} \tag{2.4}$$

where $\widetilde{\Phi}_1$ is obtained by applying the FKS projection mapping [67] to the original two-parton phase space point Φ_2. Similarly to ref. [36], we adopt $\alpha_{\mathrm{cut}} = 10^{-4}$ as our technical cutoff. The rationale behind this reweighting choice is that, in the soft-collinear limit, the ratio $\mathrm{d}\sigma^{m_t\to\infty}_{gg\to HHgg}\left(\Phi_2\right)/\mathrm{d}\sigma^{m_t\to\infty}_{gg\to HHg}\left(\widetilde{\Phi}_1\right)$ tends towards the splitting function used in the subtraction, thus reproducing the structure of the subtraction term. This ensures that the cancellation between the reweighted $gg \to HHgg$ matrix element and its counterterms, which are always evaluated with the exact top-quark mass dependence, are always locally finite in each singular limit when $\alpha_{\mathrm{cut}} \to 0$. Note that, however, for any given finite value of α_{cut}, the projected phase space point $\widetilde{\Phi}_1$ does not exactly match the point Φ_1 at which the subtraction term is evaluated. Their difference, due to IR safety, is suppressed by powers $\mathcal{O}(\alpha^n_{\mathrm{cut}})$. Consequently, in regions where $\mathcal{O}(\alpha_{\mathrm{cut}}) \sim \mathcal{O}(\mathcal{T}_0^{\mathrm{cut}}/Q)$, we expect to observe numerical discrepancies as well as instabilities in the subtractions procedure. To mitigate this, given that the smallest possible value of α_{cut} is dictated by the stability of the $gg \to HHgg$ matrix element, the value of $\mathcal{T}_0^{\mathrm{cut}}$ must be chosen to be much larger than $\alpha_{\mathrm{cut}}Q$. A more detailed discussion and validation of this choice is presented in section 3.

2.2 Comparison to other approximations

We compare our $\mathrm{FT}_{\mathrm{approx}}$ results with other approximations existing in the literature, namely the $m_t \to \infty$ approximation, corresponding to our previous results of ref. [28], and the B-proj approximation as described in ref. [36]. Below, we summarize the main features of these two approximations and refer the reader to the corresponding references for further details.

$m_t \to \infty$. This corresponds to the exact infinite top-quark mass limit, as described in ref. [28], i.e. with no rescaling or mass reweighting applied. In the literature, this approximation is often referred to as HTL, or HEFT, but in this work we reference it with $m_t \to \infty$ to avoid confusion.

JHEP09(2025)206

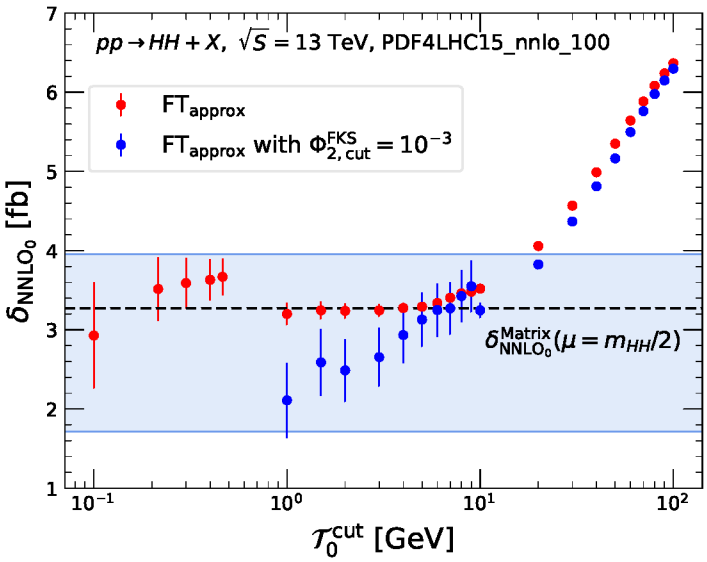

Figure 1. Relative NNLO corrections as a function of the slicing parameter $\mathcal{T}_0^{\mathrm{cut}}$, evaluated at $\sqrt{S} = 13\,\mathrm{TeV}$ and $\mu = m_{HH}/2$, using the `PDF4LHC15_nnlo_100` PDF set. The expected NNLO contribution from MATRIX, corresponding to 3.27 fb, is shown as a dashed black line.

B-proj. The B-proj approximation consists of reweighting all squared matrix elements — including those entering the hard function perturbative coefficients — using Born projected matrix elements. Specifically, the reweighting factor is given by

$$K(\Phi_n) = \frac{B_{gg\to HH}\left(\tilde{\Phi}_0(\Phi_n), m_t\right)}{B_{gg\to HH}\left(\tilde{\Phi}_0(\Phi_n), m_t \to \infty\right)}\,. \tag{2.5}$$

Notice that this provides the exact top-quark mass dependence only at LO. Starting from NLO and in the presence of further emissions, the reweighting factor is calculated on a projected kinematic $\tilde{\Phi}_0(\Phi_n)$, taken from eqs. (2.2) and (2.3) of ref. [36], and defined in ref. [68].

3 Validation of the NNLO result

We validate our results by comparing them to those in ref. [36], obtained using the MATRIX framework. As discussed in detail in ref. [28], the partonic predictions from GENEVA cannot exactly match those from purely fixed order generators such as MATRIX. This is because GENEVA includes higher order effects coming from the resummation of logarithms of the resolution variable and consequent matching to fixed order. Additionally, as discussed in section 2, we employ a different rescaling below the α_{cut} to mitigate instabilities in matrix elements evaluation in the deep IR limit. Therefore, in order to validate our predictions meaningfully, we calculate the pure NNLO correction to the cross section as done in a pure slicing calculation. This means that for each value of the resolution variable $\mathcal{T}_0^{\mathrm{cut}}$, we compute two contributions separately. Below this value, the cross section is approximated by the cumulative distribution of the resummation formula expanded at fixed order $\mathcal{O}(\alpha_s^2)$. Above the cut, we compute the exact fixed order contribution, which corresponds to the NLO

JHEP09(2025)206

correction to the $pp \to HH + j$ process, dubbed NLO_1. Schematically

$$\delta_{\text{NNLO}_0} = \Sigma_{\mathcal{O}(\alpha_s^4)} \left(\mathcal{T}_0 < \mathcal{T}_0^{\text{cut}} \right) + \delta_{\text{NLO}_1} \left(\mathcal{T}_0 > \mathcal{T}_0^{\text{cut}} \right) + \mathcal{O}\left(\mathcal{T}_0^{\text{cut}} \right) . \tag{3.1}$$

The residual $\mathcal{T}_0^{\text{cut}}$ dependence vanishes up to power corrections, since the contribution below the cut is accurate only at leading power in $\mathcal{T}_0$.

Figure 1 shows the reconstructed δ_{NNLO_0} using the $\text{FT}_{\text{approx}}$ approximation at $\sqrt{S} = 13\,\text{TeV}$ and $\mu = m_{HH}/2$, with the `PDF4LHC15_nnlo_100` PDF set [69]. Red dots represent the result of eq. (3.1), compared to the reference dashed black line at 3.27 fb, obtained by subtracting the $\text{NNLO}_{\text{FT}_{\text{approx}}}$ and the NLO MATRIX results from table 1 in ref. [36]. The light blue band around that line corresponds to the scale variation values quoted in the same reference. We find good agreement between our predictions and those obtained by MATRIX for small ($\mathcal{O}(1)\,\text{GeV}$)[1] values of $\mathcal{T}_0^{\text{cut}}$, where power corrections are suppressed. As the slicing parameter increases, deviations become visible as expected due to the growing importance of neglected higher-order terms. This reinforces the choice of a small $\mathcal{T}_0^{\text{cut}}$ for reliable and efficient resummed predictions. Note that for smaller values of $\mathcal{T}_0^{\text{cut}}$ we see deviations and even numerical instabilities, as discussed in section 2. To show the impact of this approximation, in figure 1 we additionally include, with blue dots, the effect of keeping the full top-quark mass dependence without doing any type of approximation. Due to the matrix elements instability problems mentioned earlier, however, the only way of producing any meaningful result when using the exact $gg \to HHgg$ matrix element with full top-quark mass dependence is by using a cut on the FKS variables ξ and y of the extra radiation phase space. This cut is chosen to be 10^{-3}, which is the lowest possible value we can get to before the matrix elements become completely unstable. We dub this result "$\text{FT}_{\text{approx}}$ with $\Phi_{2,\text{cut}}^{\text{FKS}} = 10^{-3}$". Notice that the result obtained in this case is only stable up to $\mathcal{T}_0^{\text{cut}} \sim 10\,\text{GeV}$, which would imply having the result afflicted by larger fiducial power corrections. This further validates our choice of approximating the top-quark mass dependence of $gg \to HHgg$ below the α_{cut} value instead of keeping the exact mass dependence but be forced to raise the technical cutoff: in this way we are lowering the power correction in zero-jettiness at the expense of including some power corrections to the exact top-quark mass.

Having validated the NNLO accuracy of our implementation, we can now move to the study of the GENEVA predictions. In figure 2 we compare with MATRIX our NNLL′+ NNLO prediction for a set of differential observables at NNLO accuracy. In particular we show the invariant mass of the Higgs boson pair (m_{HH}), their rapidity (y_{HH}) and the transverse momentum of the hardest Higgs boson ($p_T^{H_1}$). Statistical uncertainties for the MATRIX predictions were not provided, which is why they are not displayed in the main panels. Since the available results for MATRIX were obtained at $\sqrt{S} = 14\,\text{TeV}$, the GENEVA results presented in the remainder of this section are obtained with the same setup. We observe excellent agreement between the GENEVA and MATRIX results, with any discrepancies coming from the effects of the inclusion of higher order effects in GENEVA. These can play a particularly important role in the $p_T^{H_1}$ distribution, as thoroughly discussed in ref. [28]. In addition, we

[1] This is in agreement with what explained in section 2 since the average value of Q, which in our case corresponds to the invariant mass of the Higgs boson pair system, is around 500 GeV, so we expect to see numerical effects, due to a finite value of α_{cut}, until around $\mathcal{T}_0^{\text{cut}} \lesssim 0.5\,\text{GeV}$.

JHEP09(2025)206

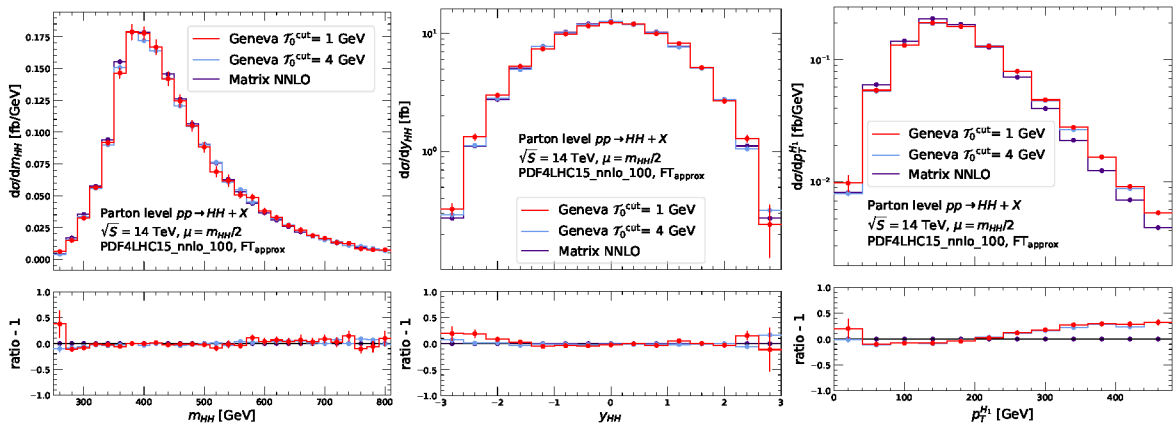

Figure 2. Comparison between the full GENEVA result for different $\mathcal{T}_0^{\rm cut}$ values (1 GeV in red and 4 GeV in light blue) and the MATRIX prediction (in purple) in the FT$_{\rm approx}$ approximation, for the invariant mass of the Higgs boson pair (left), their rapidity (centre) and the transverse momentum of the hardest Higgs boson (right). The ratio panel shows the relative differences between the predictions. Results are shown at $\sqrt{S} = 14$ TeV, $\mu = m_{HH}/2$ and using the `PDF4LHC15_nnlo_100` PDF set.

show how varying our choice of $\mathcal{T}_0^{\rm cut}$ affects differential distributions, and we see no significant impact when going from $\mathcal{T}_0^{\rm cut} = 1\,\text{GeV}$ to $\mathcal{T}_0^{\rm cut} = 4\,\text{GeV}$. Note that, in the following, we always employ $\mathcal{T}_0^{\rm cut} = 1\,\text{GeV}$ for our predictions, unless otherwise specified.

To further evidence the impact of resummation, we consider the GENEVA result at two levels: the first is NNLL′+ NNLO, corresponding to our full partonic prediction, while the second is the fixed order only contribution, obtained by running GENEVA while switching off both the resummed and the resummed-expanded contributions. Note that, strictly speaking, this latter contribution — shown in the plots for reference to illustrate the effect of resummation in the hard region — includes the $\mathcal{O}(\alpha_s^2)$ terms only for $\mathcal{T}_0 > \mathcal{T}_0^{\rm cut}$. We thus refer to it as NLO$_0$ +NLO$_1$. We report both contributions in figure 3 for the reduced $\tau_0 = \mathcal{T}_0/m_{HH}$ (left) and the Higgs boson pair transverse momentum p_T^{HH} (right). For τ_0, significant differences appear in the small-τ_0 region, where logarithmic corrections dominate and the resummation is crucial. In the lowest panel, we report the relative difference between the resummation and the resummed-expanded. As it can be seen by comparing the first and the second sub-panels, the difference between the matched result and the fixed-order only component at small τ_0 is entirely captured by the resummed term alone, since it corresponds to the difference between the resummed and the resummed-expanded. At larger values of τ_0 the resummed and the resummed-expanded cancel, as they should, since we expect the fixed order expansion to be the correct approximation in this regime.

Crucially, the fact that we perform the resummation in τ_0 has a significant impact on the p_T^{HH} distribution. Since we switch off the resummation directly in τ_0 instead of in p_T^{HH}, the effects of the resummation extend at moderately large value of p_T^{HH}, mainly because of the large size of m_{HH}. This can be clearly seen in the right panel of figure 3, where our matched result shows large differences with respect to the MATRIX sample, which are however entirely due to the presence of higher order effects from the resummation. Indeed, while we could only obtain MATRIX data for p_T values up to 500 GeV, we see that at large $p_T^{HH} \gtrsim 1000$ GeV values,

JHEP09(2025)206

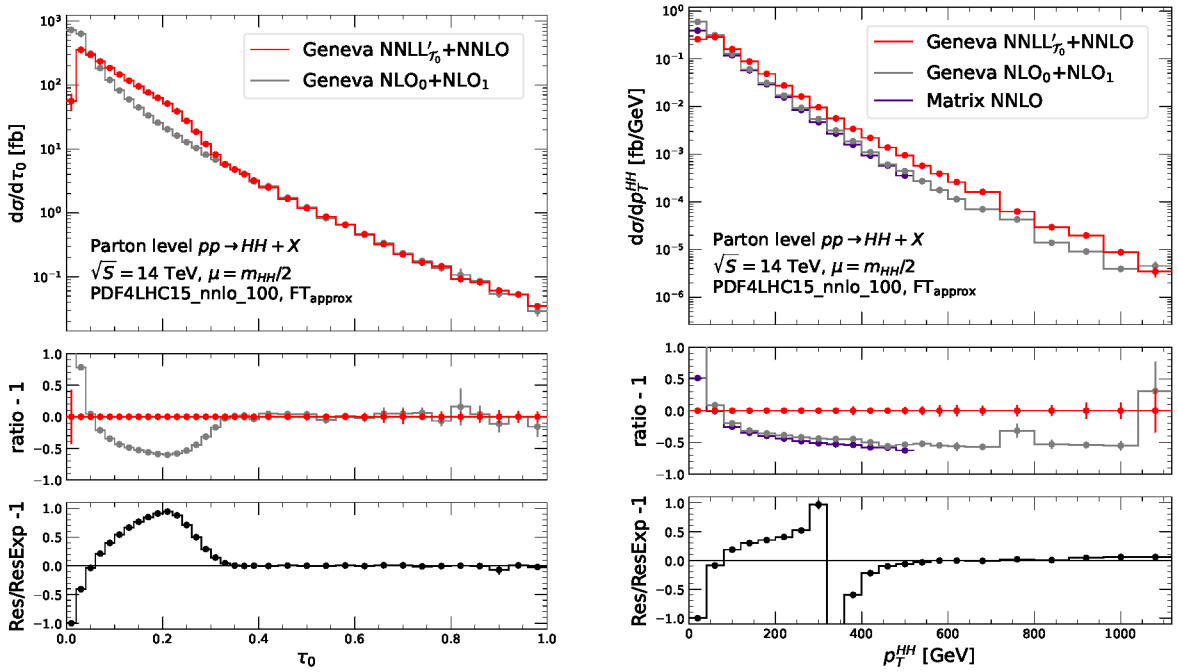

Figure 3. Impact of the resummation on the reduced τ_0 (left) and on the Higgs boson pair transverse momentum p_T^{HH} (right). The full GENEVA resummed result (in red) is compared with the corresponding fixed order prediction (in gray). For p_T^{HH}, we also report the MATRIX prediction (in purple). The top ratio panels show the relative differences between the predictions, while the lower panels show the contribution from the resummed part (i.e. the difference between the full resummed and its fixed order expansion). Results are shown at $\sqrt{S} = 14\,\text{TeV}$, $\mu = m_{HH}/2$ and using the `PDF4LHC15_nnlo_100` PDF set.

the full result and the fixed order nicely converge, as they should. A possible way to better control this behaviour would be to switch off the resummation with a hybrid scale involving both p_T and $\mathcal{T}_0$ [70], or perform a joint $p_T - \mathcal{T}_0$ resummation [71]. However, this goes beyond the scope of the present study and is left for future investigation. To conclude the section, we report in table 1 and table 2 the NNLO GENEVA inclusive cross sections (in fb) for the various top-quark mass approximations. The predictions are computed at $\mu = m_{HH}/2$ and $\mu = m_{HH}$, using the `PDF4LHC15_nnlo_100` and `PDF4LHC21_nnlo` PDF set [72], respectively.

We observe that the cross sections grow with $\sqrt{S}$, as expected from the increase of parton luminosities, in particular the gluon luminosity. This is expected because by increasing the centre-of-mass energy we are probing the PDFs at relatively smaller values of the parton longitudinal momentum fraction x. Concerning the inclusion of the top-quark mass corrections, we see that the B-proj approximation tends to overestimate the cross section compared to FT$_{\text{approx}}$, and we notice that its agreement with the FT$_{\text{approx}}$ result for total cross sections is of similar size as that of the $m_t \to \infty$ approximation. We also observe that scale uncertainties (obtained here by 3-point correlated μ_R, μ_F variations) have a typical size of $\sim 10\%$ at $\mu = m_{HH}$, consistent with previous $m_t \to \infty$ studies [28]. These uncertainties are reduced when running at $\mu = m_{HH}/2$, aligning better with ref. [36]. Future work will include 7-point scale variations for a more comprehensive uncertainty estimate.

JHEP09(2025)206

cross sections [fb]	$\sqrt{S} = 13\,\text{TeV}$	$\sqrt{S} = 13.6\,\text{TeV}$	$\sqrt{S} = 27\,\text{TeV}$
$\text{NNLO}_{\text{FT}_{\text{approx}}}$	$(31.19 \pm 0.38)^{+2.8\%}_{-5.7\%}$	$(35.17 \pm 0.41)^{+2.7\%}_{-5.5\%}$	$(134.44 \pm 3.47)^{+0.0\%}_{-2.41\%}$

Table 1. GENEVA $\text{FT}_{\text{approx}}$ inclusive cross sections for Higgs boson pair production at $\sqrt{S} = 13, 13.6$ and 27 TeV, computed at $\mu = m_{HH}/2$ The first uncertainty is statistical; the subscript/superscript indicate the 3-point inclusive scale variations. The PDF set used is `PDF4LHC15_nnlo_100`.

cross sections [fb]	$\sqrt{S} = 13\,\text{TeV}$	$\sqrt{S} = 13.6\,\text{TeV}$	$\sqrt{S} = 27\,\text{TeV}$
$\text{NNLO}_{m_t\to\infty}$	$(26.99 \pm 0.02)^{+7.2\%}_{-8.6\%}$	$(30.69 \pm 0.02)^{+7.1\%}_{-8.5\%}$	$(197.5 \pm 0.14)^{+6.8\%}_{-7.7\%}$
$\text{NNLO}_{\text{B-proj}}$	$(33.79 \pm 0.03)^{+7.2\%}_{-8.4\%}$	$(37.65 \pm 0.03)^{+7.3\%}_{-8.4\%}$	$(166.8 \pm 0.12)^{+6.7\%}_{-7.4\%}$
$\text{NNLO}_{\text{FT}_{\text{approx}}}$	$(29.11 \pm 0.20)^{+6.8\%}_{-5.2\%}$	$(32.34 \pm 0.21)^{+6.8\%}_{-5.3\%}$	$(132.9 \pm 1.20)^{+4.9\%}_{-3.4\%}$

Table 2. GENEVA inclusive cross sections for Higgs boson pair production at $\sqrt{S} = 13, 13.6$ and 27 TeV, computed at $\mu = m_{HH}$. Results are presented for the three approximations: $m_t \to \infty$, B-proj and $\text{FT}_{\text{approx}}$. The first uncertainty is statistical; the subscript/superscript indicate the 3-point inclusive scale variations. The PDF set used is `PDF4LHC21_nnlo`.

4 NNLO partonic results

In this section, we study the effects of the inclusion of top-quark mass corrections at the partonic level. In the GENEVA framework, this corresponds to a $\text{NNLL}'_{\mathcal{T}_0}$ + NNLO calculation, before the inclusion of parton shower effects. We always consider the process $pp \to HH + X$, where the leading order contribution comes solely from the gluon fusion production channel, and we require two on-shell Higgs bosons in the final state. We set the centre-of-mass energy to $\sqrt{S} = 13.6\,\text{TeV}$ to be compatible with the Run 3 of the LHC. Both the factorization and renormalization scales are dynamically chosen and set equal to the invariant mass of the Higgs boson pair, $\mu_F = \mu_R = m_{HH}$. We use the `PDF4LHC21_nnlo` parton distribution function set [72], accessed via LHAPDF6 [73], including the corresponding value of the strong coupling constant $\alpha_s(m_Z)$. The running of such coupling is performed at three-loop order by default.

We compare the three approximations presented in section 2, namely the $\text{FT}_{\text{approx}}$, B-proj and $m_t \to \infty$ calculations. We set the following input parameters

$$m_H = 125\ \text{GeV}, \qquad G_F = 1.1663787\text{e}^{-5}\ \text{GeV}^{-2}, \qquad m_t = 173\ \text{GeV} \tag{4.1}$$

to ensure consistency with the grids provided by HHGRID for the calculation of virtual corrections in $\text{FT}_{\text{approx}}$.[2] We evaluate the beam functions, needed for the resummed part of our calculation, through the `beamfunc` module of SCETLIB [75, 76]. Finally, we set our resolution cutoff as $\mathcal{T}_0^{\text{cut}} = \mathcal{T}_1^{\text{cut}} = 1\ \text{GeV}$.

Results for the three approximations are presented in figure 4, where we show predictions for the invariant mass of the Higgs boson pair m_{HH}, the rapidity of the pair y_{HH}, the transverse momentum of the hardest Higgs boson, $p_T^{H_1}$ and the distribution χ, defined as

$$\chi = \tanh\left(\frac{|y_{H_1} - y_{H_2}|}{2}\right), \tag{4.2}$$

[2] During the preparation of this manuscript we were made aware of the release of the `ggxy` library [74], which allows to vary those parameters. We plan to investigate its inclusion in GENEVA in the future.

JHEP09(2025)206

where y_{H_1,H_2} are the rapidities of the individual Higgs boson. For high energy Higgs bosons, this variable is directly related to the cosine of the scattering angle of the two bosons. Overall, we see that in most cases the B-proj prediction provides a good approximation of the full mass effects of $\mathrm{FT}_{\mathrm{approx}}$, whereas the $m_t \to \infty$ approximation fails to predict either the shape or the normalisation. This is in agreement to what is known in the literature (see for example ref. [23]). This is particularly evident for the invariant mass distribution, where the B-proj approximation reproduces a shape similar to that predicted by $\mathrm{FT}_{\mathrm{approx}}$, which serves as our best prediction. However, we observe a difference in normalization between the two, which decreases at high m_{HH} but increases at low m_{HH}, reaching roughly 20% near the production threshold. In contrast, the $m_t \to \infty$ approximation fails to capture both the normalization and the shape of the distribution, and is known to provide an unreliable description for this observable.

For the rapidity distribution y_{HH}, the differences between the B-proj and the $\mathrm{FT}_{\mathrm{approx}}$ predictions are less pronounced. The $m_t \to \infty$ result, instead, deviates significantly in shape, especially at large rapidities. Overall, the impact of top-quark mass effects on this observable is modest, especially in regions where the cross section is the largest, i.e. at central rapidities. This is consistent with expectations, as this observable is mostly driven by the PDFs, which are identical in the three approaches, and is less sensitive to the actual matrix elements.

For the transverse momentum of the hardest Higgs boson, $p_T^{H_1}$, the $m_t \to \infty$ approximation again significantly deviates in both shape and normalization. The B-proj approximation also exhibits visible discrepancies at high $p_T^{H_1}$. The low $p_T^{H_1}$ region is particularly sensitive to resummation effects, see section 3 of ref. [28]. In this case, the differences between the approximations are mostly driven by the different treatment of the $H^{(1)}$ and $H^{(2)}$ terms in the resummation formula eq. (2.1). At large $p_T^{H_1}$, discrepancies arise from configurations where one Higgs boson is very hard and recoils against a hard jet, forcing the other Higgs boson to be soft or collinear to the beam. In this situation, the projection mapping used in the B-proj approach in eq. (2.5) evaluates mass corrections with a $2 \to 2$ kinematics with back-to-back Higgs bosons, which differs significantly from the actual $2 \to 3$ or $2 \to 4$ kinematics employed by the $\mathrm{FT}_{\mathrm{approx}}$. This happens in a region where mass corrections are large, as shown by the difference between the $\mathrm{FT}_{\mathrm{approx}}$ and the $m_t \to \infty$ approximations, thus leading to relatively large effects.

In the case of the χ distribution, the differences between $\mathrm{FT}_{\mathrm{approx}}$ and $m_t \to \infty$ are less significant, indicating that top-quark mass corrections for this observables are small. However, in the region of small χ which is dominated by the recoil of the Higgs boson pair system with a hard jet, B-proj predicts consistently larger values. This discrepancy reduces only as $\chi \to 1$. The reason for the large effect at small χ is again tied to the same reasoning described for $p_T^{H_1}$. Indeed, in this region the correct kinematic configurations, which would yield small mass corrections in this observable, are those with 1 or 2 partons in the final state. However, B-proj only accounts for mass corrections in the Born-projected kinematics, thus leading to an overestimate of the mass effects.

In conclusion, the B-proj approximation better accounts for top-quark mass effects than the $m_t \to \infty$ limit, in agreement with previous studies. Nonetheless, while the reweighting procedure applied in B-proj improves the shape of some distributions, it distorts others and

JHEP09(2025)206

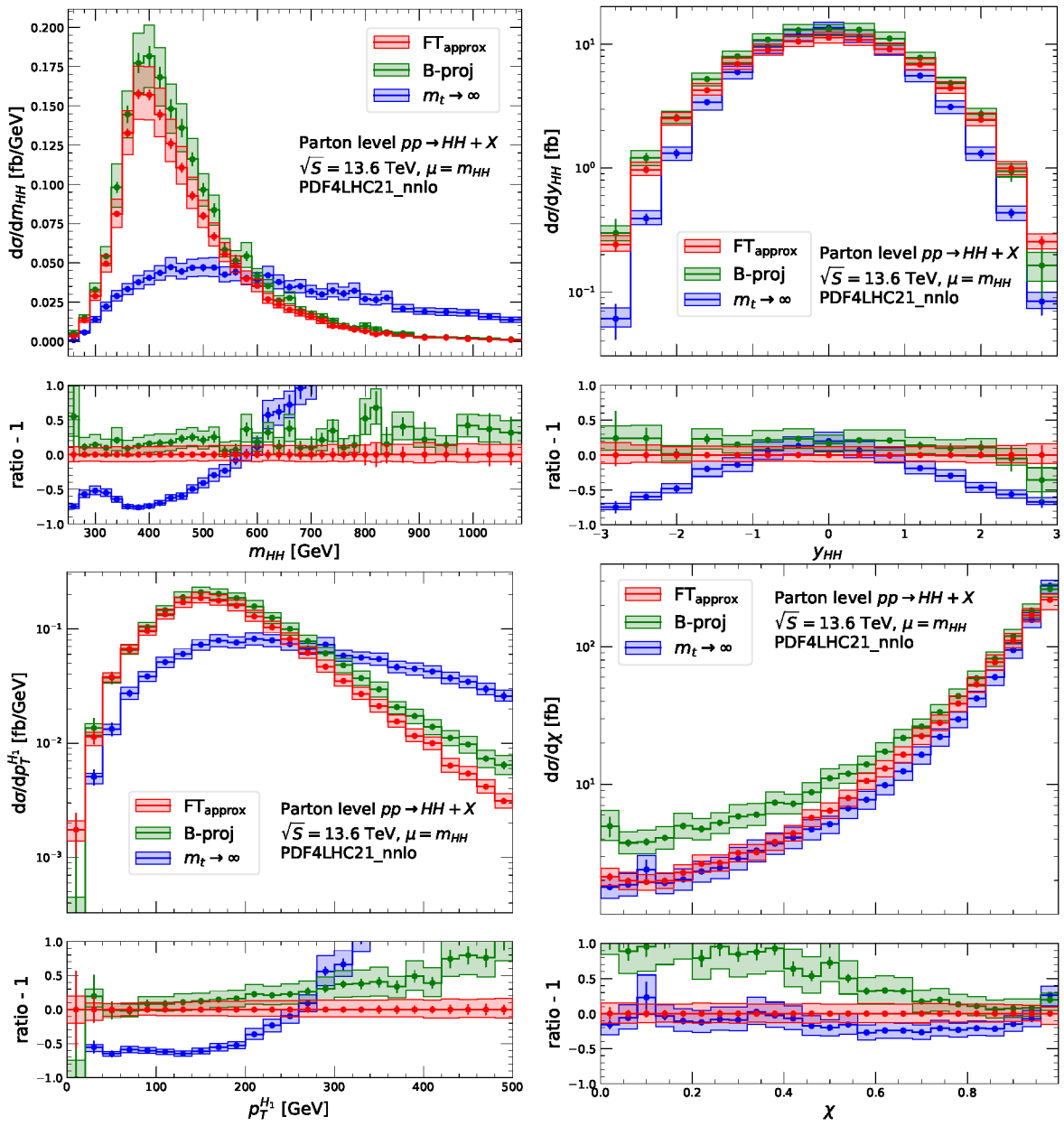

Figure 4. Comparison of partonic predictions obtained with the three top-quark mass approximations: $m_t \to \infty$ (blue), B-proj (green) and $\mathrm{FT}_{\mathrm{approx}}$ (red), shown for various differential distributions. These include the invariant mass of the Higgs boson pair (m_{HH}, top-left), the rapidity of the pair (y_{HH}, top-right), the transverse momentum of the hardest Higgs boson ($p_T^{H_1}$, bottom-left) and the χ distribution (bottom-right). Results are obtained at $\sqrt{S} = 13.6\,\mathrm{TeV}$, with central scale $\mu = m_{HH}$, using `PDFLHC21_nnlo` PDF set and 3-point scale variations.

leads to larger total cross section predictions. $\mathrm{FT}_{\mathrm{approx}}$ remains the most accurate prediction currently available, especially for shape-sensitive observables such as m_{HH} and $p_T^{H_1}$ (and therefore p_T^{HH}), whereas for more inclusive observables like y_{HH} or χ, the impact of top-quark mass corrections is comparatively mild.

JHEP09(2025)206

5 Showered results

In this section, we present fully showered results, studying the impact of mass corrections and their interplay with the parton shower (PS). We begin by noting that the parton shower performs the evolution of high-energy states down to low energy through soft and collinear emissions, which are independent of the treatment of the mass of the top-quark in the hard interactions. Consequently, we expect the effect of the parton shower to be independent of the approximation chosen for top-quark mass corrections. For this reason, while GENEVA can be interfaced to other parton showers — such as DIRE [77] and SHERPA [78], as shown in ref. [28] — we restrict our comparison to the default shower PYTHIA8 [79]. In addition, since the shower performs a leading-logarithmic (LL) resummation via its evolution, our matching procedure needs to preserve both our higher-order accuracy in the resolution variable $\mathcal{T}_0$ and the leading logarithmic one of any other variable performed by the shower. The details of how GENEVA interfaces to parton showers have been described extensively in previous works, such as ref. [80] and ref. [28], and remain unchanged from our earlier study in the $m_t \to \infty$ limit [28]. The computational setup used here is identical to that described in section 4.

We present our results in figure 5 for the three top-quark mass approximations, across four differential distributions: the invariant mass of the Higgs boson pair m_{HH}, their transverse momentum p_T^{HH}, the transverse momentum of the hardest Higgs boson, $p_T^{H_1}$ and finally the zero-jettiness $\mathcal{T}_0$. The structure of the results is the following. The main panel displays predictions after the full shower procedure, including hadronisation and multi-parton interaction (MPI) effects, but excluding hadron decays. The first ratio panel shows the relative difference of each approximation with respect to the $\mathrm{FT}_{\mathrm{approx}}$ result. The second ratio panel highlights the impact of the parton shower at parton level (i.e. without hadronisation and MPI effects), by displaying the relative difference with respect to the partonic results discussed in section 4. Finally, the third ratio panel illustrates the impact of hadronisation and MPI effects, shown relative to the parton shower results without the inclusion of hadronisation and MPI effects.

We start by noting that in the case of the Higgs boson pair mass and the p_T of the hardest Higgs boson, the inclusion of top-quark mass effects produces corrections of similar size at hadron level as at parton level, as presented in section 4. This can be seen by comparing the first ratio panel of figure 5 with the ratio panel of figure 4 for these observables. This further validates our assumption that the shower behaves independently of the treatment of top-quark mass effects in the hard interaction. Since the invariant mass of the Higgs boson pair system is an inclusive observable, for which NNLO accuracy is achieved, the parton shower has no effect due to the unitarity of the shower matching. This also holds true, in particular, for hadronisation and MPI effects, as seen in the third panel.

For the transverse momentum distributions, p_T^{HH} and p_T^{H1}, the parton shower modifies only the first few bins, with effects of approximately 5% relative to the GENEVA partonic predictions. These effects are consistent across the three approximations and are concentrated in the low-p_T region, where resummation effects dominate and are captured by the shower. Hadronisation and MPI effects, shown in the third panel, are of similar size to the pure shower effects seen in the second panel. As a consequence, they are of moderate size and concentrated in the low-p_T region. Turning to the $\mathcal{T}_0$ distribution, in the GENEVA framework

JHEP09(2025)206

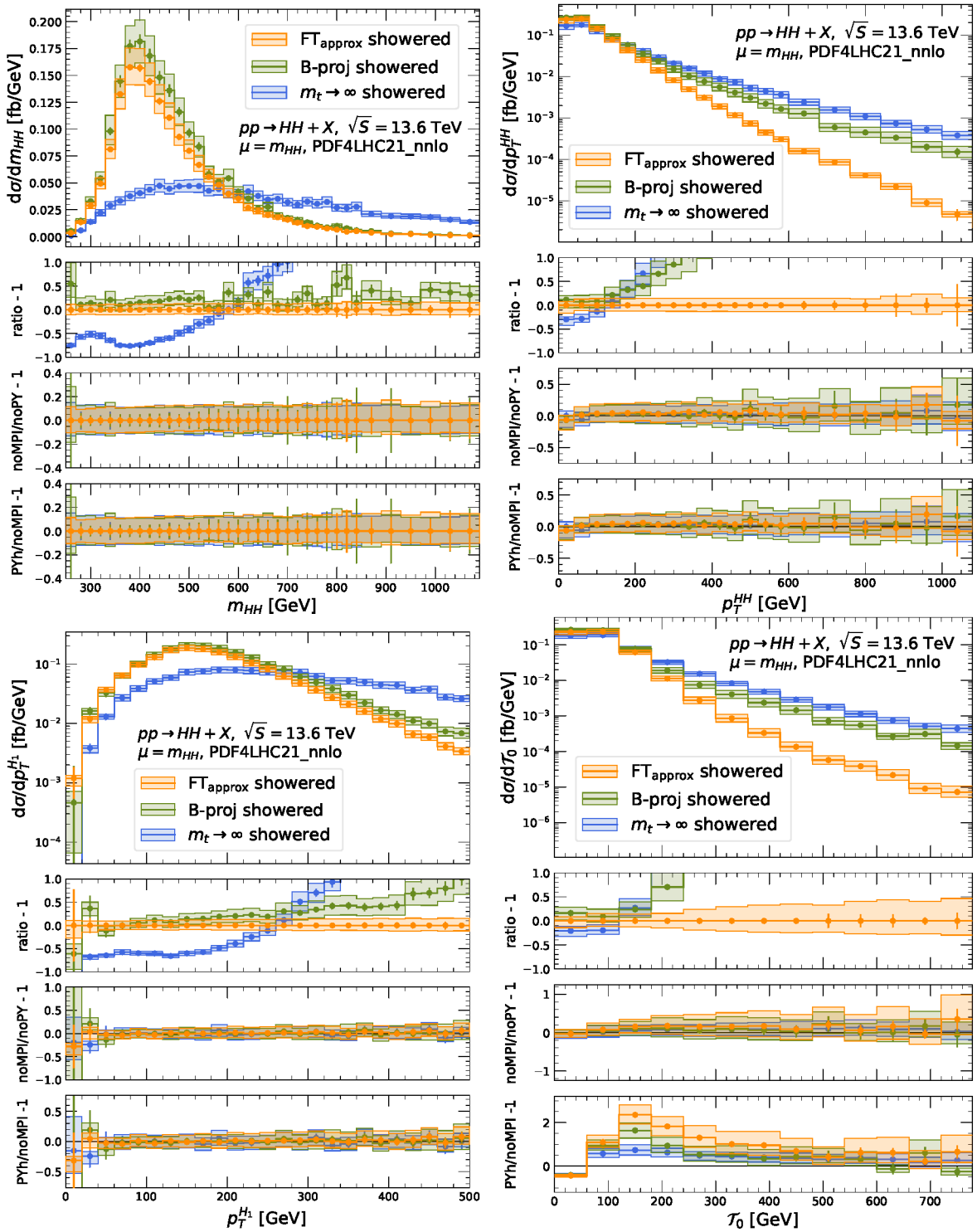

Figure 5. Comparison of showered predictions obtained with the three top-quark mass approximations: $m_t \to \infty$ (blue), B-proj (light green) and $\text{FT}_{\text{approx}}$ (dark orange), shown for various differential distributions. These include the invariant mass of the Higgs boson pair (m_{HH}, top-left), the transverse momentum of the pair system (p_T^{HH}, top-right), the transverse momentum of the hardest Higgs boson ($p_T^{H_1}$, bottom-left) and the $\mathcal{T}_0$ distribution (bottom-right). Results are obtained at $\sqrt{S} = 13.6\,\text{TeV}$, with central scale $\mu = m_{HH}$, using `PDFLHC21_nnlo` PDF set and 3-point scale variations.

JHEP09(2025)206

the matching between the partonic events and the parton shower ensures that the accuracy of each observable is, at least, as accurate as the parton shower is, which in this case is LL accurate. At the same time, we enforce that the accuracy of the resolution variable for which we perform the resummation is also not spoiled by the parton shower. The result is that any numerical modifications introduced by the shower in the small $\mathcal{T}_0$ region should not exceed the typical size of higher-order resummation effects (see e.g. figure 11 of ref. [28]). Indeed, as seen in the second panel plot, the shower does not significantly alter the distribution within statistical uncertainties. This stability is partly due to the relatively wide binning used for this observable. Lastly, we see that the impact of hadronisation and MPI for $\mathcal{T}_0$ are instead large, as shown in the third panel. This agrees with previous studies which showed the sensitivity of the zero-jettiness to such effects [81]. In particular, we see that their influence is mostly visible at low values of $\mathcal{T}_0$, where it significantly distorts the spectrum, gradually diminishing toward the tail of the distribution.

In conclusion, the qualitative impact of the default parton shower remains consistent with the results of our previous study using the $m_t \to \infty$ limit. Similar patterns are observed across all top-quark mass approximations considered in this work.

6 Conclusions

The process $gg \to HH$ plays a central role in the exploration of the Higgs sector, particularly in probing the Higgs boson self-interaction via the trilinear coupling λ_{HHH}. Given its small cross section and the complexity of the final state, precise and reliable theoretical predictions are essential not only for improving signal sensitivity, but also for disentangling potential deviations from Standard Model expectations. In this work, we have extended our previous implementation of double Higgs boson production via gluon fusion in the GENEVA framework, which was originally performed in the $m_t \to \infty$ limit, by including different approximations that account for finite top-quark mass effects. Specifically, we have added support for the so-called Born-improved (B-proj) and the $\mathrm{FT}_{\mathrm{approx}}$ approximations. The former approach reweights each event by the ratio of the full-theory (massive) to $m_t \to \infty$ Born-level squared amplitudes, requiring a projection onto Born-like kinematics. The $\mathrm{FT}_{\mathrm{approx}}$ method instead incorporates the exact top-quark mass dependence at one-loop and also in the two-loops single virtual corrections, with the correct kinematics. The remaining unknown components — namely the three-loops double-virtual and the two-loops real-virtual corrections — are rescaled using Born-level matrix elements computed with exact top-quark mass dependence.

By leveraging the GENEVA framework, we are able to produce fully differential NNLO predictions matched to a $\mathcal{T}_0$ resummation at NNLL$'$ accuracy within the SCET formalism, and further matched to a parton shower including hadronisation and multi-parton interactions (MPI). We have validated our partonic predictions against standard fixed-order results obtained with MATRIX, and we have studied the impact of the parton shower, hadronisation, and MPI on key differential observables.

This constitutes the first NNLO+PS implementation of double Higgs boson production via gluon fusion that includes top-quark mass corrections in the $\mathrm{FT}_{\mathrm{approx}}$, resulting in a realistic and flexible event generator ready to be used in experimental analyses at the LHC and future hadron colliders. To provide a framework capable of estimating all sources of theoretical

JHEP09(2025)206

uncertainties, we plan to include in future versions of our code various improvements. These will comprise top-quark mass variations, EW corrections, at least in approximate form, as well as bottom-quark mass effects, as soon as they become available.

Acknowledgments

We thank our GENEVA collaborators for their work on the code and in particular A. Broggio for discussions. We also thank J. Mazzitelli for providing the values for the MATRIX results appearing in ref. [36]. This project acknowledges funding from the European Research Council (ERC) under the European Union's Horizon 2020 research and innovation program (Grant agreements No. 714788 REINVENT and 101002090 COLORFREE) and also acknowledges support from the Deutsche Forschungsgemeinschaft (DFG) under Germany's Excellence Strategy — EXC 2121 "Quantum Universe"- 390833306. We acknowledge financial support, super-computing resources and support from ICSC — Centro Nazionale di Ricerca in High Performance Computing, Big Data and Quantum Computing — and hosting entity, funded by European Union — NextGenerationEU.

Data Availability Statement. This article has no associated data or the data will not be deposited.

Code Availability Statement. This article has no associated code or the code will not be deposited.

References

[1] CMS collaboration, *A measurement of the Higgs boson mass in the diphoton decay channel*, *Phys. Lett. B* **805** (2020) 135425 [arXiv:2002.06398] [INSPIRE].

[2] ATLAS collaboration, *Measurement of the Higgs boson mass with $H \to \gamma\gamma$ decays in 140 fb^{-1} of $\sqrt{s} = 13$ TeV pp collisions with the ATLAS detector*, *Phys. Lett. B* **847** (2023) 138315 [arXiv:2308.07216] [INSPIRE].

[3] ATLAS collaboration, *Study of the spin and parity of the Higgs boson in diboson decays with the ATLAS detector*, *Eur. Phys. J. C* **75** (2015) 476 [*Erratum ibid.* **76** (2016) 152] [arXiv:1506.05669] [INSPIRE].

[4] ATLAS collaboration, *Combination of searches for Higgs boson pair production in pp collisions at $\sqrt{s} = 13$ TeV with the ATLAS detector*, *Phys. Rev. Lett.* **133** (2024) 101801 [arXiv:2406.09971] [INSPIRE].

[5] E.W.N. Glover and J.J. van der Bij, *Higgs boson pair production via gluon fusion*, *Nucl. Phys. B* **309** (1988) 282 [INSPIRE].

[6] O.J.P. Eboli, G.C. Marques, S.F. Novaes and A.A. Natale, *Twin Higgs boson production*, *Phys. Lett. B* **197** (1987) 269 [INSPIRE].

[7] T. Plehn, M. Spira and P.M. Zerwas, *Pair production of neutral Higgs particles in gluon-gluon collisions*, *Nucl. Phys. B* **479** (1996) 46 [hep-ph/9603205] [INSPIRE].

JHEP09(2025)206

[8] D. de Florian and J. Mazzitelli, *Two-loop virtual corrections to Higgs pair production*, *Phys. Lett. B* **724** (2013) 306 [arXiv:1305.5206] [INSPIRE].

[9] D. de Florian et al., *Differential Higgs boson pair production at next-to-next-to-leading order in QCD*, *JHEP* **09** (2016) 151 [arXiv:1606.09519] [INSPIRE].

[10] L.-B. Chen, H.T. Li, H.-S. Shao and J. Wang, *Higgs boson pair production via gluon fusion at N^3LO in QCD*, *Phys. Lett. B* **803** (2020) 135292 [arXiv:1909.06808] [INSPIRE].

[11] S. Borowka et al., *Higgs boson pair production in gluon fusion at next-to-leading order with full top-quark mass dependence*, *Phys. Rev. Lett.* **117** (2016) 012001 [*Erratum ibid.* **117** (2016) 079901] [arXiv:1604.06447] [INSPIRE].

[12] S. Borowka et al., *Full top quark mass dependence in Higgs boson pair production at NLO*, *JHEP* **10** (2016) 107 [arXiv:1608.04798] [INSPIRE].

[13] G. Heinrich et al., *Electroweak corrections to Higgs boson pair production: the top-Yukawa and self-coupling contributions*, *JHEP* **11** (2024) 040 [arXiv:2407.04653] [INSPIRE].

[14] M. Bonetti, P. Rendler and W.J. Torres Bobadilla, *Two-loop light-quark electroweak corrections to Higgs boson pair production in gluon fusion*, *JHEP* **07** (2025) 024 [arXiv:2503.16620] [INSPIRE].

[15] J. Davies et al., *Higgs boson contribution to the leading two-loop Yukawa corrections to $gg \to HH$*, *JHEP* **08** (2022) 259 [arXiv:2207.02587] [INSPIRE].

[16] J. Davies, K. Schönwald, M. Steinhauser and H. Zhang, *Next-to-leading order electroweak corrections to $gg \to HH$ and $gg \to gH$ in the large-m_t limit*, *JHEP* **10** (2023) 033 [arXiv:2308.01355] [INSPIRE].

[17] H. Zhang, K. Schönwald, M. Steinhauser and J. Davies, *Electroweak corrections to $gg \to HH$: factorizable contributions*, *PoS* **LL2024** (2024) 014 [arXiv:2407.05787] [INSPIRE].

[18] J. Davies, K. Schönwald, M. Steinhauser and H. Zhang, *Analytic next-to-leading order Yukawa and Higgs boson self-coupling corrections to $gg \to HH$ at high energies*, *JHEP* **04** (2025) 193 [arXiv:2501.17920] [INSPIRE].

[19] J. Grigo, J. Hoff, K. Melnikov and M. Steinhauser, *On the Higgs boson pair production at the LHC*, *Nucl. Phys. B* **875** (2013) 1 [arXiv:1305.7340] [INSPIRE].

[20] J. Grigo, K. Melnikov and M. Steinhauser, *Virtual corrections to Higgs boson pair production in the large top quark mass limit*, *Nucl. Phys. B* **888** (2014) 17 [arXiv:1408.2422] [INSPIRE].

[21] J. Grigo, J. Hoff and M. Steinhauser, *Higgs boson pair production: top quark mass effects at NLO and NNLO*, *Nucl. Phys. B* **900** (2015) 412 [arXiv:1508.00909] [INSPIRE].

[22] R. Frederix et al., *Higgs pair production at the LHC with NLO and parton-shower effects*, *Phys. Lett. B* **732** (2014) 142 [arXiv:1401.7340] [INSPIRE].

[23] F. Maltoni, E. Vryonidou and M. Zaro, *Top-quark mass effects in double and triple Higgs production in gluon-gluon fusion at NLO*, *JHEP* **11** (2014) 079 [arXiv:1408.6542] [INSPIRE].

[24] P. Maierhöfer and A. Papaefstathiou, *Higgs boson pair production merged to one jet*, *JHEP* **03** (2014) 126 [arXiv:1401.0007] [INSPIRE].

[25] G. Heinrich et al., *NLO predictions for Higgs boson pair production with full top quark mass dependence matched to parton showers*, *JHEP* **08** (2017) 088 [arXiv:1703.09252] [INSPIRE].

[26] G. Heinrich et al., *Probing the trilinear Higgs boson coupling in di-Higgs production at NLO QCD including parton shower effects*, *JHEP* **06** (2019) 066 [arXiv:1903.08137] [INSPIRE].

[27] S. Jones and S. Kuttimalai, *Parton shower and NLO-matching uncertainties in Higgs boson pair production*, *JHEP* **02** (2018) 176 [arXiv:1711.03319] [INSPIRE].

JHEP09(2025)206

[28] S. Alioli et al., *Double Higgs production at NNLO interfaced to parton showers in GENEVA*, *JHEP* **06** (2023) 205 [arXiv:2212.10489] [INSPIRE].

[29] J. Davies and M. Steinhauser, *Three-loop form factors for Higgs boson pair production in the large top mass limit*, *JHEP* **10** (2019) 166 [arXiv:1909.01361] [INSPIRE].

[30] J. Davies, F. Herren, G. Mishima and M. Steinhauser, *Real corrections to Higgs boson pair production at NNLO in the large top quark mass limit*, *JHEP* **01** (2022) 049 [arXiv:2110.03697] [INSPIRE].

[31] J. Davies, K. Schönwald and M. Steinhauser, *Towards $gg \to HH$ at next-to-next-to-leading order: light-fermionic three-loop corrections*, *Phys. Lett. B* **845** (2023) 138146 [arXiv:2307.04796] [INSPIRE].

[32] J. Davies, K. Schönwald, M. Steinhauser and M. Vitti, *Three-loop corrections to Higgs boson pair production: reducible contribution*, *JHEP* **08** (2024) 096 [arXiv:2405.20372] [INSPIRE].

[33] Z. Hu, T. Liu and J.M. Yang, *$gg \to HH$ amplitude induced by bottom quarks at two-loop level: planar master integrals*, arXiv:2503.10051 [INSPIRE].

[34] J. Davies, K. Schönwald and M. Steinhauser, *Three-loop large-N_c virtual corrections to $gg \to HH$ in the forward limit*, *JHEP* **08** (2025) 192 [arXiv:2503.17449] [INSPIRE].

[35] D. De Florian and J. Mazzitelli, *Soft gluon resummation for Higgs boson pair production including finite M_t effects*, *JHEP* **08** (2018) 156 [arXiv:1807.03704] [INSPIRE].

[36] M. Grazzini et al., *Higgs boson pair production at NNLO with top quark mass effects*, *JHEP* **05** (2018) 059 [arXiv:1803.02463] [INSPIRE].

[37] L. Alasfar et al., *Effective field theory descriptions of Higgs boson pair production*, *SciPost Phys. Comm. Rep.* **2024** (2024) 2 [arXiv:2304.01968] [INSPIRE].

[38] L. Cadamuro, T. Ingebretsen Carlson and J. Sjölin, *Di-Higgs and effective field theory: signal reweighting beyond m_{hh}*, arXiv:2502.20976 [INSPIRE].

[39] H.-Y. Bi et al., *Electroweak corrections to double Higgs production at the LHC*, *Phys. Rev. Lett.* **132** (2024) 231802 [arXiv:2311.16963] [INSPIRE].

[40] J. Baglio et al., *Gluon fusion into Higgs pairs at NLO QCD and the top mass scheme*, *Eur. Phys. J. C* **79** (2019) 459 [arXiv:1811.05692] [INSPIRE].

[41] J. Baglio et al., *Higgs-pair production via gluon fusion at hadron colliders: NLO QCD corrections*, *JHEP* **04** (2020) 181 [arXiv:2003.03227] [INSPIRE].

[42] J. Baglio et al., *$gg \to HH$: combined uncertainties*, *Phys. Rev. D* **103** (2021) 056002 [arXiv:2008.11626] [INSPIRE].

[43] E. Bagnaschi, G. Degrassi and R. Gröber, *Higgs boson pair production at NLO in the POWHEG approach and the top quark mass uncertainties*, *Eur. Phys. J. C* **83** (2023) 1054 [arXiv:2309.10525] [INSPIRE].

[44] M. Mühlleitner, J. Schlenk and M. Spira, *Top-Yukawa-induced corrections to Higgs pair production*, *JHEP* **10** (2022) 185 [arXiv:2207.02524] [INSPIRE].

[45] M. Grazzini and H. Sargsyan, *Heavy-quark mass effects in Higgs boson production at the LHC*, *JHEP* **09** (2013) 129 [arXiv:1306.4581] [INSPIRE].

[46] R. Mueller and D.G. Öztürk, *On the computation of finite bottom-quark mass effects in Higgs boson production*, *JHEP* **08** (2016) 055 [arXiv:1512.08570] [INSPIRE].

[47] R. Grober, M. Muhlleitner, M. Spira and J. Streicher, *NLO QCD corrections to Higgs pair production including dimension-6 operators*, *JHEP* **09** (2015) 092 [arXiv:1504.06577] [INSPIRE].

JHEP09(2025)206

[48] R. Grober, M. Muhlleitner and M. Spira, *Higgs pair production at NLO QCD for CP-violating Higgs sectors*, *Nucl. Phys. B* **925** (2017) 1 [arXiv:1705.05314] [INSPIRE].

[49] D. de Florian, I. Fabre and J. Mazzitelli, *Higgs boson pair production at NNLO in QCD including dimension 6 operators*, *JHEP* **10** (2017) 215 [arXiv:1704.05700] [INSPIRE].

[50] S. Alioli, W. Dekens, M. Girard and E. Mereghetti, *NLO QCD corrections to SM-EFT dilepton and electroweak Higgs boson production, matched to parton shower in POWHEG*, *JHEP* **08** (2018) 205 [arXiv:1804.07407] [INSPIRE].

[51] G. Heinrich, S.P. Jones, M. Kerner and L. Scyboz, *A non-linear EFT description of $gg \to HH$ at NLO interfaced to POWHEG*, *JHEP* **10** (2020) 021 [arXiv:2006.16877] [INSPIRE].

[52] S. Dawson, S. Homiller and M. Sullivan, *Impact of dimension-eight SMEFT contributions: a case study*, *Phys. Rev. D* **104** (2021) 115013 [arXiv:2110.06929] [INSPIRE].

[53] D. de Florian et al., *Anomalous couplings in Higgs-boson pair production at approximate NNLO QCD*, *JHEP* **09** (2021) 161 [arXiv:2106.14050] [INSPIRE].

[54] G. Heinrich, J. Lang and L. Scyboz, *SMEFT predictions for $gg \to hh$ at full NLO QCD and truncation uncertainties*, *JHEP* **08** (2022) 079 [*Erratum ibid.* **10** (2023) 086] [arXiv:2204.13045] [INSPIRE].

[55] G. Isidori, F. Wilsch and D. Wyler, *The standard model effective field theory at work*, *Rev. Mod. Phys.* **96** (2024) 015006 [arXiv:2303.16922] [INSPIRE].

[56] S. Di Noi et al., *γ_5 schemes and the interplay of SMEFT operators in the Higgs-gluon coupling*, *Phys. Rev. D* **109** (2024) 095024 [arXiv:2310.18221] [INSPIRE].

[57] G. Heinrich and J. Lang, *Combining chromomagnetic and four-fermion operators with leading SMEFT operators for $gg \to hh$ at NLO QCD*, *JHEP* **05** (2024) 121 [arXiv:2311.15004] [INSPIRE].

[58] G. Heinrich and J. Lang, *Renormalisation group effects in SMEFT for di-Higgs production*, *SciPost Phys.* **18** (2025) 113 [arXiv:2409.19578] [INSPIRE].

[59] I.W. Stewart, F.J. Tackmann and W.J. Waalewijn, *N-jettiness: an inclusive event shape to veto jets*, *Phys. Rev. Lett.* **105** (2010) 092002 [arXiv:1004.2489] [INSPIRE].

[60] I.W. Stewart, F.J. Tackmann and W.J. Waalewijn, *Factorization at the LHC: from PDFs to initial state jets*, *Phys. Rev. D* **81** (2010) 094035 [arXiv:0910.0467] [INSPIRE].

[61] F. Cascioli, P. Maierhofer and S. Pozzorini, *Scattering amplitudes with OpenLoops*, *Phys. Rev. Lett.* **108** (2012) 111601 [arXiv:1111.5206] [INSPIRE].

[62] F. Buccioni, S. Pozzorini and M. Zoller, *On-the-fly reduction of OpenLoops*, *Eur. Phys. J. C* **78** (2018) 70 [arXiv:1710.11452] [INSPIRE].

[63] F. Buccioni et al., *OpenLoops 2*, *Eur. Phys. J. C* **79** (2019) 866 [arXiv:1907.13071] [INSPIRE].

[64] J. Davies et al., *Double Higgs boson production at NLO: combining the exact numerical result and high-energy expansion*, *JHEP* **11** (2019) 024 [arXiv:1907.06408] [INSPIRE].

[65] T. Becher and M. Neubert, *On the structure of infrared singularities of gauge-theory amplitudes*, *JHEP* **06** (2009) 081 [*Erratum ibid.* **11** (2013) 024] [arXiv:0903.1126] [INSPIRE].

[66] D. de Florian and J. Mazzitelli, *A next-to-next-to-leading order calculation of soft-virtual cross sections*, *JHEP* **12** (2012) 088 [arXiv:1209.0673] [INSPIRE].

[67] S. Frixione, Z. Kunszt and A. Signer, *Three jet cross-sections to next-to-leading order*, *Nucl. Phys. B* **467** (1996) 399 [hep-ph/9512328] [INSPIRE].

JHEP09(2025)206

[68] S. Catani, D. de Florian, G. Ferrera and M. Grazzini, *Vector boson production at hadron colliders: transverse-momentum resummation and leptonic decay*, *JHEP* **12** (2015) 047 [arXiv:1507.06937] [INSPIRE].

[69] J. Butterworth et al., *PDF4LHC recommendations for LHC run II*, *J. Phys. G* **43** (2016) 023001 [arXiv:1510.03865] [INSPIRE].

[70] P. Cal, R. von Kuk, M.A. Lim and F.J. Tackmann, *q_T spectrum for Higgs boson production via heavy quark annihilation at $N^3LL'+aN^3LO$*, *Phys. Rev. D* **110** (2024) 076005 [arXiv:2306.16458] [INSPIRE].

[71] G. Lustermans, J.K.L. Michel, F.J. Tackmann and W.J. Waalewijn, *Joint two-dimensional resummation in q_T and 0-jettiness at NNLL*, *JHEP* **03** (2019) 124 [arXiv:1901.03331] [INSPIRE].

[72] PDF4LHC Working Group collaboration, *The PDF4LHC21 combination of global PDF fits for the LHC run III*, *J. Phys. G* **49** (2022) 080501 [arXiv:2203.05506] [INSPIRE].

[73] A. Buckley et al., *LHAPDF6: parton density access in the LHC precision era*, *Eur. Phys. J. C* **75** (2015) 132 [arXiv:1412.7420] [INSPIRE].

[74] J. Davies, K. Schönwald, M. Steinhauser and D. Stremmer, *ggxy: a flexible library to compute gluon-induced cross sections*, arXiv:2506.04323 [INSPIRE].

[75] G. Billis, M.A. Ebert, J.K.L. Michel and F.J. Tackmann, *A toolbox for q_T and 0-jettiness subtractions at N^3LO*, *Eur. Phys. J. Plus* **136** (2021) 214 [arXiv:1909.00811] [INSPIRE].

[76] M.A. Ebert et al., *SCETlib: a C++ package for numerical calculations in QCD and soft-collinear effective theory*, DESY-17-099, http://scetlib.desy.de.

[77] S. Höche and S. Prestel, *The midpoint between dipole and parton showers*, *Eur. Phys. J. C* **75** (2015) 461 [arXiv:1506.05057] [INSPIRE].

[78] Sherpa collaboration, *Event generation with Sherpa 2.2*, *SciPost Phys.* **7** (2019) 034 [arXiv:1905.09127] [INSPIRE].

[79] T. Sjöstrand et al., *An introduction to PYTHIA 8.2*, *Comput. Phys. Commun.* **191** (2015) 159 [arXiv:1410.3012] [INSPIRE].

[80] S. Alioli et al., *Drell-Yan production at NNLL'+NNLO matched to parton showers*, *Phys. Rev. D* **92** (2015) 094020 [arXiv:1508.01475] [INSPIRE].

[81] S. Alioli, C.W. Bauer, S. Guns and F.J. Tackmann, *Underlying event sensitive observables in Drell-Yan production using GENEVA*, *Eur. Phys. J. C* **76** (2016) 614 [arXiv:1605.07192] [INSPIRE].

JHEP09(2025)206